

## Theory of fluorescence in photonic crystals

Nipun Vats\* and Sajeev John

*Department of Physics, University of Toronto, 60 St. George Street, Toronto, Ontario M5S 1A7, Canada*

Kurt Busch<sup>†</sup>

*Institute für Theorie der Kondensierten Materie, Universität Karlsruhe, 76128 Karlsruhe, Germany*

(Received 13 November 2001; published 21 March 2002)

We present a formalism for the description of fluorescence from optically active materials embedded in a photonic crystal structure possessing a photonic band gap or pseudogap. An electromagnetic field expansion in terms of Bloch modes of the crystal is used to develop the equations for fluorescence in terms of the local density of photon modes available to the emitting atoms in either the high or low dielectric regions of the crystal. We then obtain expressions for fluorescence spectra and emission dynamics for luminescent materials in photonic crystals. The validity of our formalism is demonstrated through the calculation of relevant quantities for model photon densities of states. The connection of our calculations to the description of realistic systems is discussed. We also describe the consequences of these analyses on the accurate description of the interaction between radiative systems and the electromagnetic reservoir within photonic crystals.

DOI: 10.1103/PhysRevA.65.043808

PACS number(s): 42.50.Ct, 42.70.Qs, 32.50.+d

### I. INTRODUCTION

Photonic crystals (PCs) are periodic dielectric structures that use a carefully engineered combination of microscopic scattering resonances from individual elements of the periodic array and Bragg scattering from the dielectric lattice to strongly modify the dispersion (energy-momentum) relation of light [1]. From a fundamental perspective, these materials are of interest for their ability to drastically alter the nature of the propagation of light [2,3]. Of even greater current interest is the potential that such materials offer for significantly improving the emission characteristics of active optical devices [4], such as diodes, optical switches, and low power laser systems.

The most drastic modification of light propagation, and of the associated ability to modify the emission properties of active optical devices, occurs when a PC is designed so that the propagation of light within it is prohibited in all three directions for a continuous range of frequencies. This propagation-free frequency range is known as a photonic band gap (PBG) [3,4]. An active material with a free space radiative transition that lies deep inside a PBG will be unable to emit a photon when placed inside a PBG material; instead, a photon-atom bound state is formed [5]. For transitions near the edge of a PBG, the emission dynamics will be modified relative to free space, due to the restricted number of photon modes available at the band edge [6]. The resulting non-Markovian atom-field interaction has been predicted to give rise to a number of quantum optical phenomena, such as rapid multiatom switching with low quantum noise [7], laserlike collective atomic emission [8], and atomic states that can be readily generated and protected from processes that

would serve to decohere the system [9]. Additionally, localized and extended defects can be engineered in the otherwise optically empty PBG in order to waveguide light [10], and to produce strongly localized states of light that can serve as extremely high- $Q$  microcavities for microlaser and cavity QED applications [11,12].

Since the first demonstration of a PBG material operating at microwave frequencies [13], experimental efforts have been focused on creating such materials at the optical–near-IR frequencies relevant to optical communications. To produce a full PBG typically requires a connected network of high index material containing a periodic array of air voids [43]. The periodicity of these voids should be comparable to the relevant wavelength of light. Clearly, these conditions are difficult to achieve on the micron length scale of optical crystals. However, in the past two years, advances in microlithography [14], and in the fabrication of self-organizing colloidal systems [15] have produced materials with strong pseudogaps in the optical. More recently, materials that suggest a full photonic band gap at frequencies in the near-IR have been produced [10,16]. In particular, an inverse opal PBG material [16] can be constructed by infiltrating the voids in a colloidal synthetic opal crystal (grown by self-assembly) with a dielectric material (such as Si), and then etching away the initial colloidal template. The result is an optical PBG material that can be made highly ordered over hundreds of lattice constants, and that can eventually be produced in a cost-effective manner.

Recently, there has been considerable experimental work on radiative emission from active materials embedded in optical PCs with photon propagation pseudogaps, i.e., materials that prohibit photon propagation in only certain directions [17–20]. These studies are important precursors to future studies in PBG materials, so that one might optimize the emission properties of active materials in the latter structures. Furthermore, certain types of quantum optical phenomena, such as improved optical switching [7], in fact do not require a complete band gap, but only a strong

\*Present address: Woodrow Wilson School of Public and International Affairs, Princeton University, Princeton, NJ 08544-1013. Email address: nvats@princeton.edu

<sup>†</sup>Email address: kurt@tkm.physik.uni-karlsruhe.de

pseudogap. This along with the fact that pseudogap structures are simpler to fabricate than those with a full PBG means emission studies of pseudogap structures are of interest in their own right for device applications.

It is the aim of this work to provide an efficient formalism for interfacing realistic calculations of the photon dispersion relation (and the associated spatial distribution of the EM modes) in a PC with calculations of the emission properties of active media embedded in these materials. In particular, we treat the phenomenon of fluorescence from a dilute distribution of active elements (e.g., atoms, molecules) placed within the high or low dielectric fraction of a PC. The study of fluorescence from within a PC is of considerable interest for a number of reasons. Firstly, it provides an important tool for the characterization of a PC. Active elements within the crystal may couple to modes that are inaccessible from outside the crystal due to the mismatch in symmetry between Bloch modes within the crystal and external plane waves [21,22]. As a result, fluorescence from a PC may prove to be a more reliable means of determining the presence of a full PBG than reflection and transmission experiments [18,19]. Secondly, our formalism permits an evaluation of qualitative treatments of radiative emission from a photonic crystal based on model photon dispersion relations. Furthermore, our method enables a quantitative description of the interaction between an atom and the electromagnetic modes available in a PC, which is central to the description of quantum optical phenomena in these materials.

The outline of this paper is as follows. In Sec. II we develop a quantum description of the atom-field interaction in a realistic PC in terms of the natural (Bloch) modes of a periodic crystal. In Sec. III we derive the integro-differential equation describing fluorescence from active media. In the process, we introduce the concepts of the projected local density of states, and the orientationally averaged local density of states, which describe the local electromagnetic fields seen by radiating atomic dipoles in this system. Section IV derives the expressions for fluorescence spectra and dynamics starting from the local photon density of states, including a detailed treatment of the Lamb shift in a PC. We then test our formalism on idealized models of the dispersion relation in a PC in Sec. V. Finally, in Sec. VI we give a qualitative discussion of how our formalism may be applied to interpret actual fluorescence experiments in PCs.

## II. ATOM-FIELD COUPLING IN A PHOTONIC CRYSTAL

We aim to describe the fluorescence spectrum and emission dynamics of an active material placed in either the high or low index region of a photonic crystal. Physical realizations of such a system include, for example, dilute solutions of fluorescent organic dyes in the void regions [20] and luminescent rare-earth ions embedded in the dielectric backbone of an air-dielectric crystal [23]. The active material is modeled as a collection of two-level atoms situated at random positions. These atoms are, furthermore, assumed to be present in a sufficiently low density so as to eliminate the possibility of collective coherent emission. The differences between realistic active elements and our somewhat ideal-

ized system are discussed in Sec. VI.

The Hamiltonian for an electron in an electromagnetic field may in general be written in the form:

$$H_{el} = \frac{1}{2m_e} [\mathbf{p} - e\mathbf{A}(\mathbf{r})]^2 - e\Phi(\mathbf{r}). \quad (2.1)$$

$\mathbf{p}$  and  $m_e$  are the momentum and mass of the atomic transition electron, respectively, and  $\mathbf{A}(\mathbf{r})$  and  $\phi(\mathbf{r})$  are, respectively, the electromagnetic vector and scalar potentials. Using Maxwell's equations and their relations to the associated potential functions, the equations of motion for the classical scalar potential  $\Phi$  and the vector potential  $\mathbf{A}$  can be written as [24]

$$[\nabla^2 \mathbf{A}(\mathbf{r}, t) - \nabla[\nabla \cdot \mathbf{A}(\mathbf{r}, t)]] - \frac{\epsilon_p(\mathbf{r})}{c^2} \left[ \frac{\partial^2 \mathbf{A}(\mathbf{r}, t)}{\partial t^2} + \frac{\partial}{\partial t} \nabla \Phi(\mathbf{r}, t) \right] = 0, \quad (2.2)$$

$$\begin{aligned} \nabla \epsilon(\mathbf{r}) \cdot \nabla \Phi(\mathbf{r}, t) + \epsilon(\mathbf{r}) \nabla^2 \Phi(\mathbf{r}, t) + \nabla \epsilon(\mathbf{r}) \cdot \frac{\partial \mathbf{A}(\mathbf{r}, t)}{\partial t} \\ + \epsilon(\mathbf{r}) \frac{\partial}{\partial t} \nabla \cdot \mathbf{A}(\mathbf{r}, t) = 0, \end{aligned} \quad (2.3)$$

where the dielectric permittivity is given by  $\epsilon(\mathbf{r}) = \epsilon_p(\mathbf{r})\epsilon_0$ , and in the present study is assumed to be linear and frequency-independent in the frequency range of interest. The spatially varying dielectric function  $\epsilon_p(\mathbf{r})$  describes the periodic modulation of the dielectric constant within a photonic crystal,  $\epsilon_p(\mathbf{r}) = \epsilon_p(\mathbf{r} + \mathbf{R})$ , where  $\mathbf{R}$  is a vector of the direct Bravais lattice,  $\mathbf{R} = \sum_i n_i \mathbf{a}_i$ ,  $n_j \in I$ , the  $\mathbf{a}_j$  being basis vectors of the periodic lattice. To simplify our expression for  $\mathbf{A}$ , we choose to work in a gauge in which  $\Phi = 0$ . Equation (2.2) reveals that this condition can be satisfied provided that:

$$\nabla \cdot [\epsilon(\mathbf{r})\mathbf{A}] = 0. \quad (2.4)$$

The consequences of this constraint are discussed below.

A classical theory for the electromagnetic field in a photonic crystal based on the above equations is developed in detail in Refs. [24] and [25]. The classical equations may be quantized in the usual manner [24,26]; the appropriately quantized solution of Eq. (2.2) for the vector potential may be expanded in the general form

$$\hat{\mathbf{A}}(\mathbf{r}, t) = \sum_{\mathbf{k}, \sigma} C_{\mathbf{k}} \{ \mathbf{A}_{\mathbf{k}, \sigma}(\mathbf{r}) \hat{a}_{\mathbf{k}, \sigma}(t) + \mathbf{A}_{\mathbf{k}, \sigma}^*(\mathbf{r}) \hat{a}_{\mathbf{k}, \sigma}^\dagger(t) \}, \quad (2.5)$$

where  $\hat{a}_{\mathbf{k}, \sigma}(t) \equiv \hat{a}_{\mathbf{k}, \sigma}(0) e^{-i\omega_{\mathbf{k}} t}$  is the annihilation operator for a field mode with wave vector  $\mathbf{k}$  and with polarization  $\sigma = 1, 2$ , and satisfies the boson commutation relation  $[\hat{a}_{\mathbf{k}, \sigma}, \hat{a}_{\mathbf{k}, \sigma}^\dagger] = \delta_{\mathbf{k}, \mathbf{k}'} \delta_{\sigma, \sigma'}$ . The mode functions  $\mathbf{A}_{\mathbf{k}, \sigma}(\mathbf{r})$  may in general be any complete set of basis functions spanning the region under consideration. In free space, where there is complete translational symmetry, it is natural to choose as

basis functions simple plane waves,  $\mathbf{A}_{\mathbf{k},\sigma}(\mathbf{r}) = e^{i\mathbf{k}\cdot\mathbf{r}}\mathbf{e}_{\mathbf{k},\sigma}$ ,  $\mathbf{e}_{\mathbf{k},\sigma}$  being a unit vector in the direction of the polarization state  $\sigma$  for a given wave vector  $\mathbf{k}$ . In a photonic crystal, the periodicity of the dielectric breaks this full translational symmetry. As a result, the field seen by an active atom varies from point to point within a unit cell of the crystal [27]. One may express  $\hat{\mathbf{A}}(\mathbf{r})$  at a specific point using a plane-wave basis; however, such an approach would not elucidate or take advantage of the symmetry properties of the periodic crystal. It is therefore highly advantageous to use a basis of Bloch modes, which satisfy the Bloch-Floquet theorem,

$$\mathbf{A}_{\mathbf{k}}(\mathbf{r}+\mathbf{R}) = e^{i\mathbf{k}\cdot\mathbf{R}}\mathbf{A}_{\mathbf{k}}(\mathbf{r}), \quad (2.6)$$

as we may then conveniently restrict our attention to a single Wigner-Seitz cell of the lattice. If we then adopt a reduced zone scheme for  $\mathbf{k}$  [28], we may write the vector potential in a photonic crystal as

$$\begin{aligned} \hat{\mathbf{A}}(\mathbf{r},t) = & \sum_n \int_{BZ} \frac{d^3k}{(2\pi)^3} \sqrt{\frac{\hbar}{2\epsilon_0\omega_{n,\mathbf{k}}V}} \{ \mathbf{A}_{n,\mathbf{k}}(\mathbf{r}) \hat{a}_{n,\mathbf{k}}(t) \\ & + \mathbf{A}_{n,\mathbf{k}}^*(\mathbf{r}) \hat{a}_{n,\mathbf{k}}^\dagger(t) \}, \end{aligned} \quad (2.7)$$

where  $V$  is the volume of a unit cell of the lattice,  $n$  is the energy band index in the first Brillouin zone, and the wave-vector integration is over each band in this region of  $\mathbf{k}$  space. Mode functions labeled by  $n$  are henceforth understood to be Bloch modes of the crystal. Unlike in free space, different polarization states for a given wave vector are not necessarily degenerate in energy. Therefore the band index  $n$  also counts the polarization states for a given wave vector  $\mathbf{k}$ .

From Eq. (2.1), we see that the quantized interaction Hamiltonian of the atom and field for an atomic electron at position  $\mathbf{r}_0$  is given by

$$\hat{H}_{int} = -\frac{e}{2m_e} [\hat{\mathbf{p}} \cdot \hat{\mathbf{A}}(\mathbf{r}_0) + \hat{\mathbf{A}}(\mathbf{r}_0) \cdot \hat{\mathbf{p}}]. \quad (2.8)$$

In this expression, we have neglected the term involving  $A^2$  in the Hamiltonian (2.1), as it describes photon-photon interactions, which are negligible at low energies. Note that in general the electron momentum and the vector potential do not commute:  $[\hat{\mathbf{A}}(\mathbf{r}), \hat{\mathbf{p}}] = i\hbar \nabla \cdot \hat{\mathbf{A}}(\mathbf{r})$ . However, in a spatially homogeneous dielectric, Eq. (2.4) reduces to the condition  $\nabla \cdot \hat{\mathbf{A}} = 0$ , and we recover the well-known  $\hat{\mathbf{p}} \cdot \hat{\mathbf{A}}$  form of the minimal coupling Hamiltonian. Clearly, this is not the case in a periodic dielectric. We may, however, assume that the electromagnetic field varies little over the spatial extent of the electronic wave function, thus allowing us to keep only the dipole contribution of the electronic charge distribution. As pointed out by Kweon and Lawandy [24], when such an approximation is valid, we may then evaluate the vector potential at the position of the atomic center of mass. Since the electron mass is very small compared to that of the atomic nucleus, this is equivalent to evaluating  $\hat{\mathbf{A}}$  at the atomic nucleus, whose motion is independent of the electronic motion. We may then write

$$\hat{H}_{int} \simeq -\frac{e}{m_e} \hat{\mathbf{p}} \cdot \hat{\mathbf{A}}(\mathbf{r}_0), \quad (2.9)$$

where  $\mathbf{r}_0$  is now understood to be the position of the atomic nucleus. Alternatively, we may simply note that the spatial variation in the dielectric constant occurs over the length scale of the lattice constant of the crystal, which is orders of magnitude larger than the spatial extent of the individual active atoms. As a result, we may treat  $\epsilon(\mathbf{r})$  as a constant over the length scale of the active elements, thus validating Eq. (2.9).

At this point, we proceed to rewrite the interaction term in the form  $\hat{\mathbf{D}} \cdot \hat{\mathbf{E}}$  [29] in the electric dipole approximation, where  $\hat{\mathbf{D}}$  is the usual electric dipole operator, and  $\hat{\mathbf{E}}$  is the electric field operator obtained from Eq. (2.7). We note that in principle one may derive the  $\hat{\mathbf{D}} \cdot \hat{\mathbf{E}}$  form of the interaction directly from the Hamiltonian (2.1), without recourse to the approximation scheme presented here, thereby avoiding issues relating to the acausal nature of the vector potential (see, e.g., Ref. [30]). Nevertheless, our approach results in the correct form for the atom-field coupling.

In a rotating-wave approximation, the full Hamiltonian for a two-level atom and the electromagnetic field in a photonic crystal can now be written as

$$\begin{aligned} H_{tot} = & \frac{\hbar}{2} \omega_{21} \sigma_z + \hbar \sum_{\mu} \omega_{\mu} a_{\mu}^{\dagger} a_{\mu} \\ & + i\hbar \sum_{\mu} (g_{\mu} a_{\mu}^{\dagger} \sigma_{-} - g_{\mu}^{*} \sigma_{+} a_{\mu}). \end{aligned} \quad (2.10)$$

The index  $\mu$  labels the energy band and wave vector of a given field mode,  $\mu \equiv \{n, \mathbf{k}\}$ , and the  $\sigma_j$  ( $j = +, -$ ) are the usual Pauli operators for a two-level atom with a (bare) atomic resonance frequency  $\omega_{21}$ . We have also dropped the circumflexes denoting operators, as in what follows the distinction between operators and ordinary functions should be self-evident. The position-dependent atom-field mode coupling constants  $g_{\mu}$  are given by

$$g_{\mu}(\mathbf{d}, \mathbf{r}_0) \equiv g_{\mu} = \omega_{21} d_{21} \sqrt{\frac{1}{2\hbar \epsilon_0 \omega_{\mu} V}} \mathbf{d} \cdot \mathbf{E}_{\mu}^*(\mathbf{r}_0), \quad (2.11)$$

where  $d_{21}$  and  $\mathbf{d}$  are, respectively, the magnitude and the direction unit vector of the dipole matrix element for the atomic transition. Whereas the condition  $\nabla \cdot \mathbf{A} = 0$  in free space implies that the plane-wave modes are transverse ( $\mathbf{k} \cdot \mathbf{A} = 0$ ), condition (2.4) for a photonic crystal does not necessarily give transverse polarization states for Bloch modes.

### III. EQUATIONS OF MOTION

We wish to analyze the atomic emission in a Schrödinger equation formalism [6,31]. Atom-field interactions that involve more than one photon are more easily (and often necessarily) described by a density matrix or by Heisenberg operator equations, and much of our analysis can be carried

over to such systems; see Sec. IV C. In the single photon sector, the system wave function for a two-level atom with dipole moment  $d_{21}\mathbf{d}$  is

$$|\Psi\rangle = b_2(\mathbf{d}, \mathbf{r}_0, t)|2, \{0\}\rangle + \sum_{\mu} b_{1,\mu}(\mathbf{d}, \mathbf{r}_0, t)|1, \{\mu\}\rangle e^{-i\Delta_{\mu}t}. \quad (3.1)$$

$b_2(\mathbf{d}, \mathbf{r}_0, t)$  and  $b_{1,\mu}(\mathbf{d}, \mathbf{r}_0, t)$  label the probability amplitudes for the excited atom plus an electromagnetic vacuum state, and a deexcited atom with a single photon in mode  $\mu$ , respectively, at a given position  $\mathbf{r}_0$  of a Wigner-Seitz cell in a photonic crystal;  $\Delta_{\mu} = \omega_{\mu} - \omega_{21}$ . In a frame that is corotating with the bare atomic resonance frequency,  $\omega_{21}$ , Eq. (3.1) along with the Hamiltonian (2.10) give the equations of motion for the amplitudes,

$$\frac{d}{dt}b_2(\mathbf{d}, \mathbf{r}_0, t) = - \sum_{\mu} g_{\mu} b_{1,\mu}(\mathbf{d}, \mathbf{r}_0, t) e^{-i\Delta_{\mu}t}, \quad (3.2)$$

$$\frac{d}{dt}b_{1,\mu}(\mathbf{d}, \mathbf{r}_0, t) = g_{\mu} b_2(\mathbf{d}, \mathbf{r}_0, t) e^{i\Delta_{\mu}t}. \quad (3.3)$$

Formally integrating Eq. (3.3) and substituting the solution into Eq. (3.2), we arrive at an equation for the excited state amplitude,

$$\frac{d}{dt}b_2(\mathbf{d}, \mathbf{r}_0, t) = - \int_0^t G(\mathbf{d}, \mathbf{r}_0, t-t') b_2(\mathbf{d}, \mathbf{r}_0, t') dt'. \quad (3.4)$$

$G(\mathbf{d}, \mathbf{r}_0, t-t')$  is a time delay Green function, or memory kernel, which describes the mean effect of the electromagnetic vacuum on the atomic system [8] at position  $\mathbf{r}_0$ ; it is defined as

$$G(\mathbf{d}, \mathbf{r}_0, \tau) \equiv \Theta(\tau) \sum_{\mu} |g_{\mu}(\mathbf{d}, \mathbf{r}_0)|^2 e^{-i\Delta_{\mu}\tau}. \quad (3.5)$$

Here  $\Theta(\tau)$  is the Heaviside step function, which ensures that  $G(\mathbf{d}, \mathbf{r}_0, \tau) = 0$  for  $\tau < 0$ , as required by causality considerations.

Making explicit the band and wave-vector contributions to the wave-vector sum, Eq. (3.5) becomes

$$\begin{aligned} G(\mathbf{d}, \mathbf{r}_0, \tau) &= \Theta(\tau) \alpha \sum_n \int_{1\text{BZ}} d\mathbf{k} \frac{e^{-i\Delta_{n,\mathbf{k}}\tau}}{\omega_{n,\mathbf{k}}} |\mathbf{d} \cdot \mathbf{E}_{n,\mathbf{k}}(\mathbf{r}_0)|^2 \\ &= \Theta(\tau) \alpha \sum_n \int_0^{\infty} d\omega \frac{e^{-i(\omega - \omega_{21})\tau}}{\omega} \\ &\quad \times \int_{1\text{BZ}} d\mathbf{k} \delta(\omega - \omega_{n,\mathbf{k}}) |\mathbf{d} \cdot \mathbf{E}_{n,\mathbf{k}}(\mathbf{r}_0)|^2, \end{aligned} \quad (3.6)$$

where  $\alpha = \omega_{21}^2 d_{21}^2 / 16\hbar \epsilon_0 \pi^3$ , and the  $\mathbf{k}$ -space integration is over the first Brillouin zone. Here we have added a frequency integration over a Dirac  $\delta$  function, which does not affect the value of  $G(\mathbf{d}, \mathbf{r}_0, \tau)$ . The frequency integral is de-

fined only over positive frequencies, as there are no negative energy photon modes. Note that Eq. (3.6) does not contain within it a conventional total density of states (DOS), which counts the number of modes available at a given frequency,

$$N(\omega) \equiv \sum_n \int_{1\text{BZ}} d\mathbf{k} \delta(\omega - \omega_{n,\mathbf{k}}). \quad (3.7)$$

Such a DOS fails to account for either (i) the relative orientation of the atomic dipole and a given field mode, or (ii) the local contribution of the  $\mu$ th mode at the position  $\mathbf{r}_0$ . It is therefore more useful to consider a projected local density of states, defined as

$$N_p(\mathbf{d}, \mathbf{r}_0, \omega) = \sum_n \int_{1\text{BZ}} d\mathbf{k} \delta(\omega - \omega_{n,\mathbf{k}}) |\mathbf{d} \cdot \mathbf{E}_{n,\mathbf{k}}(\mathbf{r}_0)|^2. \quad (3.8)$$

For a specific atom, or for coherent, collective emission from a group of atoms (e.g., lasing or superradiant emission), one must explicitly consider the relative orientation of the atomic dipole and the various Bloch modes in Eq. (3.8). In the case of fluorescence, however, we have a collection of independently emitting atoms with essentially random dipole orientations. As a result, in order to describe the ‘‘mean’’ emission characteristics of the system, we average  $\mathbf{d}$  over all solid angles, giving a factor of  $1/3$ . We may further introduce a distribution function,  $\rho(\mathbf{r})$ , which describes the density of fluorescing atoms at a given point in the crystal. We shall assume that the atomic distribution is the same for each unit cell. Performing an average over both dipole orientation and the atomic distribution within the crystal, we obtain an expression for the fluorescence Green function,

$$\begin{aligned} G_f(\tau) &\equiv \langle G(\mathbf{d}, \mathbf{r}, \tau) \rangle_{\mathbf{r}, \theta} \\ &= \Theta(\tau) \beta \int_{\text{WSC}} d\mathbf{r} \frac{\rho(\mathbf{r})}{N_e} \int_0^{\infty} d\omega \frac{N_l(\mathbf{r}, \omega)}{\omega} e^{-i(\omega - \omega_{21})\tau}, \end{aligned} \quad (3.9)$$

where, after performing the angular integration, the local density of states (LDOS) is defined as

$$\begin{aligned} N_l(\mathbf{r}, \omega) &\equiv \frac{3}{4\pi} \langle N_p(\mathbf{d}, \mathbf{r}, \omega) \rangle_{\theta} \\ &= \sum_n \int_{1\text{BZ}} d\mathbf{k} \delta(\omega - \omega_{n,\mathbf{k}}) |\mathbf{E}_{n,\mathbf{k}}(\mathbf{r})|^2. \end{aligned} \quad (3.10)$$

$\langle \rangle_{\mathbf{r}}$  and  $\langle \rangle_{\theta}$  are used to denote the spatial and orientational averages, respectively, and in Eq. (3.9), we have absorbed all numerical factors into the prefactor  $\beta = \omega_{21}^2 d_{21}^2 / 12\hbar \epsilon_0 \pi^2$ . The spatial integration is performed over the density distribution function for the active atoms in a Wigner-Seitz cell, such that  $\int d\mathbf{r} \rho(\mathbf{r}) = N_e$ , the total number of active atoms within this unit cell. The replacement of  $G(\mathbf{r}, \tau)$  by  $G_f(\tau)$  in Eq. (3.4) gives the equation of motion for the probability amplitude of the excited state population in fluorescent emis-

sion; we denote this normalized fluorescence amplitude by  $b_f(t)$ . The resulting fluorescence equation is then

$$\frac{d}{dt}b_f(t) = - \int_0^t G_f(t-t')b_f(t')dt'. \quad (3.11)$$

As discussed in Refs. [27] and [32], it is the local density of states (3.10) that one must evaluate in order to determine the electromagnetic modes in a given frequency range available to the active atoms in fluorescence, as the Bloch mode of a periodic dielectric for a given band  $n$  tends to reside preferentially in either the high or low dielectric region of the crystal. Different modes may therefore have very different spatial distributions, and accordingly can couple very differently to an active atom at a given position in the crystal. We note that Eq. (3.10) corresponds to the local radiative DOS of Ref. [27]. However, because we have made a field expansion in terms of the natural Bloch modes of the crystal, in our case the distinction between a local DOS and a local radiative DOS does not arise. The relation between the LDOS and the total DOS is given by the expression

$$N(\omega) = \int_{W_{SC}} d\mathbf{r} \epsilon(\mathbf{r}) N_l(\mathbf{r}, \omega), \quad (3.12)$$

which shows that for a small dielectric modulation in the crystal, which implies a weak interaction between the dielectric and the electromagnetic field, the total DOS can provide a reasonable description of the field at any point in the crystal. Clearly, such a condition is not satisfied by a crystal exhibiting a strong pseudogap or a full photonic band gap [33].

#### IV. EVALUATION OF FLUORESCENCE SPECTRA AND DYNAMICS

Below, we describe the method of calculation of experimentally measurable quantities from fluorescence experiments for a given LDOS. For convenience, we shall presently consider the case of a single radiating atom in each unit cell at the position  $\mathbf{r}_0$ , such that

$$\rho(\mathbf{r}) = \delta(\mathbf{r} - \mathbf{r}_0),$$

and  $N_e = 1$ . The fluorescence Green function (3.9) is then

$$G_{f_1}(\tau) = \Theta(\tau) \beta \int_0^\infty d\omega \frac{N_l(\omega)}{\omega} e^{-i(\omega - \omega_{21})\tau}, \quad (4.1)$$

where it is understood that  $N_l(\omega)$  is evaluated at the position  $\mathbf{r}_0$ . This simplification is made only to make our subsequent analysis more transparent; spatial averages over more complicated atomic density distributions may be introduced in a straightforward manner, due to the linear nature of the averaging process. Because of the complexity of calculating  $N_l(\mathbf{r}, \omega)$  throughout the active fraction of the crystal, it may in fact prove to be more practical to evaluate  $G_{f_1}(\tau)$  at a few representative points within a unit cell. We note that for a

crystal comprised of many unit cells, we are still justified in performing an average over dipole orientations, as the dipole orientations of the single atoms in each unit cell are uncorrelated.

Central to our analysis is the Fourier transform of the probability amplitude  $b_f(t)$ , which is given by

$$\tilde{b}_f(\Omega - \omega_{21}) \equiv \int_{-\infty}^{\infty} dt' b_f(t') e^{i(\Omega - \omega_{21})t'}. \quad (4.2)$$

The factor of  $e^{-i\omega_{21}t}$  in the integrand accounts for the fact that  $b_f(t)$  has been defined in a rotating frame in Eq. (3.11). Evaluating Eq. (4.2), we obtain

$$\tilde{b}_f(\Omega - \omega_{21}) = [\tilde{G}_{f_1}(\Omega - \omega_{21}) - i(\Omega - \omega_{21})]^{-1}, \quad (4.3)$$

in which  $\tilde{G}(\Omega)$  is the Fourier transform of the memory kernel (4.1);

$$\tilde{G}_{f_1}(\Omega - \omega_{21}) = \beta \int_{-\infty}^{\infty} d\tau' \int_0^\infty d\omega \Theta(\tau') \frac{N_l(\omega)}{\omega} e^{i(\Omega - \omega)\tau'}. \quad (4.4)$$

Changing the order of integration and performing the time integration in Eq. (4.4) yields

$$\begin{aligned} \tilde{G}_{f_1}(\Omega - \omega_{21}) &= \beta \int_0^\infty d\omega \frac{N_l(\omega)}{\omega} \left[ \pi \delta(\Omega - \omega) + i\text{P} \left( \frac{1}{\Omega - \omega} \right) \right] \\ &= \beta \left[ \pi \frac{N_l(\Omega)}{\Omega} + i\text{P} \int_0^\infty d\omega \frac{N_l(\omega)}{\omega(\Omega - \omega)} \right]. \end{aligned} \quad (4.5)$$

P denotes a Cauchy principal-value integral. We may thus re-express Eq. (4.3) in the form

$$\begin{aligned} \tilde{b}_f(\Omega - \omega_{21}) &= \left\{ \beta \pi \frac{N_l(\Omega)}{\Omega} - i \left[ \Omega - \omega_{21} \right. \right. \\ &\quad \left. \left. - \beta \text{P} \int_0^\infty d\omega \frac{N_l(\omega)}{\omega(\Omega - \omega)} \right] \right\}^{-1}. \end{aligned} \quad (4.6)$$

We see that the last term on the right-hand side (rhs) of this expression appears to shift the bare atomic frequency, and is in fact the source of the atomic Lamb shift, as described below.

##### A. The Lamb shift

As is well known from the theory of free space spontaneous emission, the dressing of an atom by virtual photons leads to a shift of its bare atomic resonant frequency [29]. In photonic crystals, the modified electromagnetic vacuum near a photonic band gap or pseudogap may produce an anomalous Lamb shift [5]. In particular, calculations for simple model systems have suggested that near the edge of a full gap, the strong dressing of an atomic system by real, Bragg reflected photons may be sufficiently strong so as to split a

formerly degenerate atomic level into a doublet that is repelled from the band edge both into and out of the gap. This effect could then give rise to fractional localization effects and vacuum Rabi oscillations in the atomic emission dynamics [6]. The possibility of detecting such effects in realistic photonic crystals is discussed in Sec. VB.

The energy eigenvalue equation for the dressed atomic frequency(ies) is given by an equation for the real part of the poles of  $\tilde{b}_f(\Omega)$  after analytic continuation to a complex frequency space; the imaginary part is responsible for atomic decay. From Eq. (4.6), the implicit eigenvalue equation for the dressed atomic frequency  $\tilde{\omega}_{21}$  is

$$\tilde{\omega}_{21} - \omega_{21} = \beta \mathcal{P} \int_0^\infty d\omega' \frac{N_I(\omega')}{\omega'(\tilde{\omega}_{21} - \omega')}, \quad (4.7)$$

where the principal-value integration is assumed when the dressed frequency lies in the allowed electromagnetic continuum,  $N_I(\omega) \neq 0$ .

Because the density of states for large frequencies should approach the free space DOS, i.e.,  $N_I(\omega) \propto \omega^2$  for large  $\omega$ , we see that the right-hand side of this equation is formally divergent. A complete treatment of this divergence would require a relativistic quantum field-theoretic approach; instead we appeal to the nonrelativistic prescription of Bethe [34]: The right-hand side of Eq. (4.7) can be written in the alternative form

$$\begin{aligned} & \beta \mathcal{P} \int_0^\infty d\omega' \frac{N_I(\omega')}{\omega'(\tilde{\omega}_{21} - \omega')} \\ &= \tilde{\omega}_{21} \beta \mathcal{P} \int_0^\infty d\omega' \frac{N_I(\omega')}{(\omega')^2(\tilde{\omega}_{21} - \omega')} \\ & \quad - \beta \int_0^\infty d\omega' \frac{N_I(\omega')}{(\omega')^2}. \end{aligned} \quad (4.8)$$

The last term in this equation is linearly divergent, and is related to the fact that the bare electronic mass is also dressed by the electromagnetic field. It can thus be removed from the equation if we include a mass renormalization counterterm in our initial Hamiltonian. This leaves only the first term, which is at most only logarithmically divergent. This latter divergence can be treated by introducing a cutoff in the frequency integration at the electron's Compton frequency  $\omega_e$ , as higher energy components would probe the relativistic structure of the electron and can therefore be neglected in our analysis. The Lamb shift is thus given by the solution(s) to the equation [35]

$$\tilde{\omega}_{21} - \omega_{21} = \tilde{\omega}_{21} \beta \mathcal{P} \int_0^{\omega_e} d\omega' \frac{N_I(\omega')}{(\omega')^2(\tilde{\omega}_{21} - \omega')}. \quad (4.9)$$

In free space, the atom-field coupling strength, given by  $\beta$ , is weak ( $\ll \tilde{\omega}_{21}$ ), and  $N_I(\omega)$  is a smoothly varying function. As a result, we may assume that the pole of  $\tilde{b}_f(\Omega)$  is

only slightly shifted from its undressed value, which amounts to setting  $\tilde{\omega}_{21} = \omega_{21}$  on the right-hand side of Eq. (4.9). This pole approximation, along with the free space DOS,  $N(\omega) = \omega^2/c^3$ , gives the usual Wigner-Weisskopf result for the free space Lamb shift,  $\delta_{Lamb} = -\omega_{21} \beta \ln(\omega_e/\omega_{21})/c^3$ . Near a photonic band gap,  $\beta$  is unchanged from its free space value; however,  $N_I(\omega)$  can in principle vary sufficiently strongly as to modify the Wigner-Weisskopf picture. We therefore retain the full expression (4.9) in our consideration of the Lamb shift in photonic crystals. Finally, we note that because of the explicit functional dependence of the Lamb shift on the bare atomic frequency and the DOS in a photonic crystal, we cannot *a priori* transform the equations of motion for the fluorescence dynamics to a rotating frame at a constant Lamb-shifted frequency, as is commonly done in free space. It is for this reason that we have chosen to work in a rotating frame at the bare atomic frequency.

## B. Emission spectra

The fluctuation or emission spectrum for fluorescent emission as a function of frequency,  $\Omega$ , is given by the Wiener-Khinchine relation [29],

$$\begin{aligned} S(\Omega) &\equiv 2 \operatorname{Re} \left\{ \int_{-\infty}^{\infty} dt' b_f(t') e^{i(\Omega - \omega_{21})t'} \right\} \\ &= 2 \operatorname{Re}[\tilde{b}_f(\Omega - \omega_{21})]. \end{aligned} \quad (4.10)$$

Extracting the real part of Eq. (4.6), the emission spectrum (4.10) for an arbitrary DOS is given by [31]

$$S(\Omega) = 2\beta\pi \frac{\Omega N_I(\Omega)}{[\beta\pi N_I(\Omega)]^2 + \Omega^2(\Omega - \tilde{\omega}_{21})^2}. \quad (4.11)$$

Here, we have again denoted the Lamb-shifted atomic frequency by  $\tilde{\omega}_{21} \equiv \omega_{21} + \beta \mathcal{P} \int_0^\infty d\omega [N_I(\omega)/\omega(\Omega - \omega)]$ . We see explicitly that the form of the emission spectrum is completely determined by the LDOS in the crystal, and by the position of the (dressed) atomic transition frequency. The emission spectrum thus defined corresponds to the total spectrum obtained by considering the radiation emitted into all directions from the active medium.

## C. Emission dynamics and electromagnetic reservoir correlations

The dynamics of fluorescent emission are given by the evolution of the excited state atomic population,  $|b_f(t)|^2$ . Because our input parameter is the LDOS of the crystal, we wish to evaluate  $b_f(t)$  from the inverse Fourier transform of  $b_f(\Omega)$ , i.e.,

$$\begin{aligned}
b_f(t) &= \frac{1}{2\pi} \int_{-\infty}^{\infty} d\omega \tilde{b}_f(\omega - \omega_{21}) e^{-i(\omega - \omega_{21})t} \\
&= \frac{1}{2\pi} \int_{-\infty}^{\infty} d\omega e^{-i(\omega - \omega_{21})t} \left[ \beta \pi \frac{N_I(\omega)}{\omega} \Theta(\omega) \right. \\
&\quad \left. + i\omega \beta P \int_0^{\infty} d\omega' \frac{N_I(\omega')}{(\omega')^2(\omega - \omega')} \right. \\
&\quad \left. - i(\omega - \omega_{21}) \right]^{-1}, \quad (4.12)
\end{aligned}$$

where we have transformed back to a rotating frame, and we have made explicit the fact that  $N_I(\omega)$  is defined only for positive frequencies by the use of the step function,  $\Theta(\omega)$ . From this expression, we see that for  $t=0$ , the fact that  $N_I(\Omega) \propto \Omega^2$  for large frequencies means that the memory kernel will be logarithmically divergent. However, we are only interested in the behavior of this function on the time scale of the atomic dynamics; this is, in general, much longer than the natural time scale in Eq. (3.9), which is set by the atomic resonance frequency,  $\omega_{21}$ . We therefore impose a high-frequency cutoff on Eq. (4.12) for  $t=0$  without any loss of information on the time scale of atomic emission. We choose to apply a smooth cutoff of the form  $e^{-\omega^2/\omega_c^2}$ , and we choose  $\omega_c$  such that our result is insensitive to perturbations about this choice of cutoff (in practical terms,  $\omega_c \approx 3\omega_{21}$ ). This transform is then well defined for a given  $N_I(\omega)$ , and can be efficiently calculated by standard Fourier integral methods. We note that in contrast to the Lamb shift, which probes the high-frequency behavior of the LDOS and the associated virtual photon contribution, the presence of the phase factor  $e^{-i(\omega - \omega_{21})t}$  in Eq. (4.12), coupled with the fact that the remaining argument of the integrand falls off at large frequencies implies that the emission dynamics are determined only by the LDOS the vicinity of the atomic frequency.

We may also evaluate the memory kernel  $G(\tau)$ , which may also be referred to as the temporal autocorrelation function for the electromagnetic reservoir. As previously mentioned, this function plays a central role in the description of the atom-field interaction and therefore allows us to characterize the nature of this interaction in a given photonic crystal. From Eq. (3.9),  $G(\tau)$  may be defined in terms of  $N_I(\omega)$  as

$$G(\tau) = \Theta(\tau) \beta \int_0^{\infty} d\omega \frac{N_I(\omega)}{\omega} e^{-i(\omega - \omega_{21})\tau}. \quad (4.13)$$

Upon the evaluation of Eq. (4.13), the resulting function  $G(\tau)$  may be used to evaluate the emission dynamics by direct integration of Eq. (3.11) in the time domain. This method is numerically more straightforward than the evaluation of Eq. (4.12); however, it is considerably more computationally intensive, as it requires that we explicitly integrate over all previous values of  $b_f(t')$  in order to obtain  $b_f(t)$ .

## V. FLUORESCENCE FOR MODEL PHOTON DENSITIES OF STATES

We now apply the methods of Sec. IV to simple models of the photon dispersion relation and of the associated density of states as a test of our method. We explicitly consider three cases: free space, a model DOS for an anisotropic photonic band edge, and a model DOS for a pseudogap in a photonic crystal. For simplicity, the DOS in these models is chosen to be position independent. Nevertheless, in light of the computational complexity of calculating a realistic LDOS, such idealized models provide an invaluable means of developing a qualitative and quantitative understanding of the atom-field interaction in a photonic crystal. While the chosen models provide an analytic form of the DOS, we note that our method does not require that such an analytic form exists, in contrast to previous attempts to describe the spontaneous emission of an atom in a PC [6,36].

### A. Free space

As is well known, the free space photon dispersion relation is linear and isotropic, i.e.,  $\omega_{\mathbf{k}} = c|\mathbf{k}|$ . The corresponding DOS is therefore given by  $N(\omega) = 2\omega^2/c^3$ , where the factor of 2 has been included to account for the two photon polarizations that are degenerate in energy. The Lamb shift for this case has been discussed in Sec. IV A, and is given approximately by  $\delta_{Lamb} = \omega_{21}\beta \ln(\omega_e/\omega_{21})/c^3 = \gamma \ln(\omega_e/\omega_{21})/2\pi$ , where  $\omega_e \approx m_e c^2/\hbar$ , and  $m_e$  is the electron mass. For  $\gamma = 10^8 \text{ sec}^{-1}$  and  $\omega_{21} = 10^{15} \text{ sec}^{-1}$ , we arrive at a value of  $\delta_{Lamb} = 2.2 \times 10^8 \text{ sec}^{-1}$ . Since  $\delta_{Lamb}$  is essentially constant, we incorporate it into our definition of the atomic resonant frequency  $\omega_{21}$ .

The exact spectrum evaluated from Eq. (4.11) is given by

$$S(\Omega) = 2 \frac{a\Omega}{(a\Omega)^2 + (\Omega - \omega_{21})^2}, \quad (5.1)$$

where  $a = \gamma/2\omega_{21}$ . For atomic transitions in the optical and near-ir regions, we have  $\gamma/\omega_{21} \sim 10^{-7}$ , so that we may approximate by the usual free space Lorentzian emission spectrum with a linewidth given by  $\gamma$ ,

$$S(\Omega) = \frac{\gamma}{(\gamma/2)^2 + (\Omega - \omega_{21})^2}, \quad (5.2)$$

in agreement with the result obtained in the Markovian approximation. As expected, the corresponding emission dynamics show the decay of the upper atomic state to be highly exponential in nature, with a decay rate of  $\gamma$ . Both in free space and in the case of a PC, our results are obtained in the absence of a Markovian memory kernel [29].

### B. Anisotropic band-edge model

In order to describe the atom-field interaction near a photonic band-edge, we consider an anisotropic effective mass model for the photonic dispersion [8,36]. The band edge of a

three-dimensional photonic crystal is associated with a set of  $n$  high symmetry points on the surface of the first Brillouin zone of the crystal, whose positions in reciprocal space are given by the vectors  $\mathbf{k}_0^i$ ,  $i=1, n$ . For example, in an inverse opal PBG material, the band edge for the PBG between the 8th and 9th bands occurs at the  $W$  point, which is highly degenerate.

We expand the photon dispersion relation about the upper band edge,  $\omega_u$ , to quadratic order in  $\mathbf{k}$ , giving

$$\omega_{\mathbf{k}} = \omega_u + A |\mathbf{k} - \mathbf{k}_0^i|^2. \quad (5.3)$$

We note that by choosing to expand the dispersion relation about the upper band edge, we are describing field modes that reside predominantly in the void region of the crystal (the ‘‘air’’ band) [39], a fact that is borne out by an explicit calculation of the LDOS [32]. Accordingly, this expansion is applicable to the description of emission from active elements in the void regions at frequencies near the upper band edge. In this case, we may neglect the influence of the lower band. Similar considerations may be used to motivate an expansion about the lower band edge for active elements in the dielectric fraction of the crystal.

In a PBG material, the degree of curvature of the dispersion relation near the band edge will be strongly dependent on the specific structure and dielectric material being considered, as well as on the direction of the expansion about the band edge [37]. Therefore, it is more accurate to express the expansion coefficient  $A$  as a tensor quantity, to be determined from a microscopic calculation of the dispersion near a band edge; this is, however, beyond the scope of the present work. For our purposes, we shall therefore assume that  $A$  is a scalar constant, a condition that is satisfied exactly for crystal geometries in which the band-edge wave vector possesses cubic symmetry within the Brillouin zone [5], and is otherwise a reasonable approximation for the dispersion relation near a band edge after averaging over all directions. From Eq. (5.3), the DOS can be written as

$$N(\omega) = \sqrt{\frac{\omega - \omega_u}{A^3}} \Theta(\omega - \omega_u). \quad (5.4)$$

The  $(\omega - \omega_u)^{1/2}$  dependence of  $N(\omega)$  is characteristic of a three-dimensional phase space [38], and is in agreement with the band edge LDOS computed for an inverse opal PBG material [32]. The physical quantities we wish to compute require the evaluation of the product  $\beta N(\omega)$ , which may be expressed as

$$\beta N(\omega) \approx \omega_u^{3/2} \beta_A^{1/2} \sqrt{\omega/\omega_u - 1}.$$

Here,  $\beta_A$  is the characteristic frequency for band-edge dynamics in the anisotropic model, and is given by

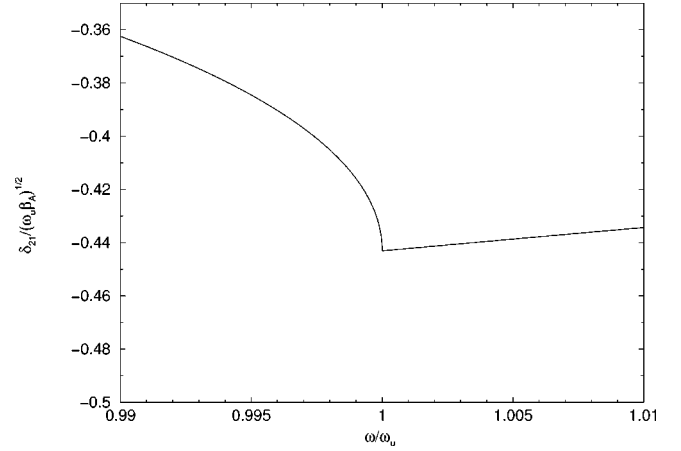


FIG. 1. Plot of the Lamb shift as a function of frequency near an anisotropic band edge.

$$\beta_A^{1/2} = \frac{\omega_{21}^2 d_{21}^2}{8 \hbar \epsilon_0 \omega_u (\pi A)^{3/2}}. \quad (5.5)$$

From this expression, it is clear that the determination of the frequency and time scales for band-edge fluorescence will depend on an accurate determination of the expansion parameter  $A$  for a specific PBG material. The value  $\beta_A$  may thus be deduced from a careful calculation of the LDOS in the vicinity of the band edge of a given crystal. In the present work, we shall instead rescale the relevant quantities to the frequency scale  $\beta_A$ ; a preliminary estimate in Ref. [40], however, suggests that  $\beta_A$  should fall within the range of  $0.01\gamma < \beta_A < 10\gamma$ . The ambiguity inherent to this simple model demonstrates the need for a more realistic calculation of the LDOS in order to obtain a quantitative evaluation of the atom-field interaction in a PBG material.

The Lamb shift computed from Eq. (4.9) is shown in Fig. 1. We see that the shift is frequency dependent near the band edge, showing that the standard Wigner-Weisskopf approach is not applicable. In order to obtain a quantitative estimate of the Lamb shift at the band edge, we take the representative values of  $\gamma = 10^8 \text{ sec}^{-1}$ ,  $\beta_A = 0.01\gamma$  and  $\omega_u = 1 \times 10^{15} \text{ sec}^{-1}$ , which gives a value of  $\delta_{Lamb}(\omega_u) \approx 2 \times 10^9 \text{ sec}^{-1}$ ; this value is an order of magnitude larger than the free space Lamb shift. The accuracy of our calculation is, however, compromised by the fact that we have neglected the contribution of the lower band edge to the frequency integration. Additionally, the density of states for our model does not accurately take into account the structure of the DOS at frequencies well above the band edge. Nevertheless, our model captures the qualitative behavior of the Lamb shift, and should give a rough estimate of its band-edge value in a real PBG material.

The spectrum is derived from Eq. (4.11), and has the form

$$S(\omega) \sim \sqrt{\frac{\beta_A}{\omega_u}} \frac{2b \sqrt{\omega/\omega_u - 1}}{\omega_u b^2 (\omega/\omega_u - 1) (\beta_A/\omega_u) + (\omega/\omega_u)^2 \{[\omega - \omega_{21} + \delta_{Lamb}(\omega/\omega_u)]/\omega_u\}^2} \Theta(\omega/\omega_u - 1). \quad (5.6)$$

Here,  $b = 3\sqrt{\pi}/2$ . We see from this expression that the functional form of the Lamb shift contribution ensures that the spectrum is finite for all values of the bare atomic frequency,  $\omega_{21}$ , including the value  $\omega_{21} = \omega_u$ . This spectrum is plotted in Fig. 2. As expected, there is no emission of radiation in the forbidden band gap, and the emission goes to zero at the photonic band edge due to the absence of electromagnetic modes at  $\omega_u$ . We see that the amount of emitted radiation increases as the atomic resonance frequency is moved farther out of the gap, and there is radiation emitted even for  $\omega_{21}$  inside the gap. The form of the spectrum is non-Lorentzian, implying a nonexponential decay of the excited atomic state population. We, however, find that for larger detunings of  $\omega_{21}$  into the allowed band the spectrum approaches a Lorentzian shape centered at the atomic frequency that is cut off for frequencies in the gap. We observe a long spectral tail that extends far into the allowed electromagnetic continuum for all detunings of  $\omega_{21}$  near the band edge. This is a result of the  $\sqrt{\omega - \omega_u}$  dependence of the DOS, which results in a slow decay of the spectrum at higher frequencies when compared with free space. We expect that this spectral tail would be diminished when using a more accurate model of the DOS, in which the slowly increasing square root dependence of the DOS does not extend throughout the allowed band.

We now turn our attention to the dynamics of the population of the upper atomic state for an initially inverted active medium. The excited-state population is plotted in Fig. 3 for various values of the detuning of the atomic transition frequency from the band edge. We observe a nonzero population in the steady state for  $\omega_{21}$  within the gap. This is a result of the fractional localization of the emitted radiation about the atom in the steady state. For  $\omega_{21}$  at the band edge, or within the allowed band, we find that the excited state population decays to zero in the steady state. The population decay becomes exponential for sufficiently large detunings into the continuum of modes, with a decay rate proportional to the density of states, as one would expect from a perturbative solution for atomic decay. We note that the degree of local-

ization of the upper state population for  $\omega_{21}$  within the gap is influenced by the DOS in the continuum of modes, even for atomic transitions well within the gap, as the relevant integrals extend over all frequencies. This accounts for the absence of a completely localized state (excited state population of unity) for  $\omega_{21}$  deep in the gap within our model. Our results for the band-edge dynamics are very similar to those of Yang and Zhu [36], which were obtained by the method of Laplace transforms. However, there are quantitative differences, likely owing to the fact that their treatment used an approximate form of the memory kernel (4.13) associated with the DOS for the anisotropic model. Here, we have made no such approximation. As discussed in Sec. IV C, the fact that the emission dynamics probe only the DOS near the atomic resonant frequency implies that the results we have obtained should not be greatly affected by the inaccurate high-frequency limit of the DOS in our band-edge model.

Finally, it is straightforward to show that  $G_f(t-t')$  evaluated from Eq. (4.13) for the DOS (5.4) has the form

$$G_f(t-t') = \omega_u^{3/2} \beta_A^{1/2} e^{i(\delta + \omega_u)(t-t')} \left\{ \frac{e^{-i[\omega_u(t-t') + \pi/4]}}{\sqrt{\omega_u(t-t')}} - \sqrt{\pi} [1 - \Phi(\sqrt{i\omega_u(t-t')})] \right\}, \quad (5.7)$$

where  $\Phi(x)$  is the error function,  $\Phi(x) = (2/\sqrt{\pi}) \int_0^x e^{-t^2} dt$ . This result is in agreement with the previously derived result for the anisotropic model [8]. This may be compared with the free space Markovian result,  $G_f(t-t') = (\gamma/2) \delta(t-t')$ , which implies that the atomic system in free space has no memory of its state at previous times on the time scale of atomic emission. We therefore observe that the nonzero temporal correlations contained in Eq. (5.7) are the source of the deviations from the Markovian behavior for atomic emission. In general,  $G_f(t-t')$ , or where appropriate,  $G(\mathbf{d}, \mathbf{r}_0, \tau)$  [Eq. (3.6)] fully characterize the interaction between an ac-

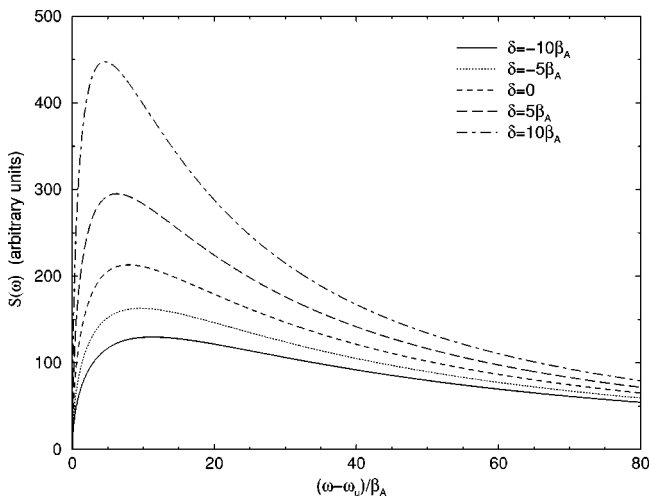


FIG. 2. Emission spectrum near an anisotropic band edge for various values of the detuning of the atomic frequency from the band-edge frequency,  $\delta = \omega_{21} - \omega_u$ .

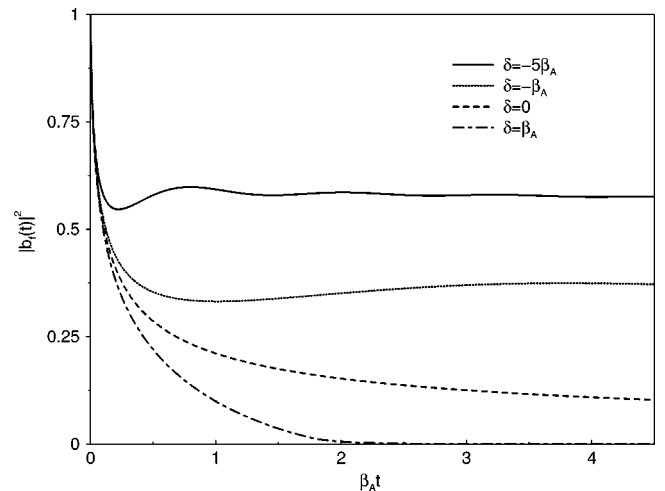


FIG. 3. Temporal evolution of the excited state population for an initially excited two-level atom near an anisotropic band-edge for various values of the detuning of the atomic frequency from the band-edge frequency,  $\delta = \omega_{21} - \omega_u$ .

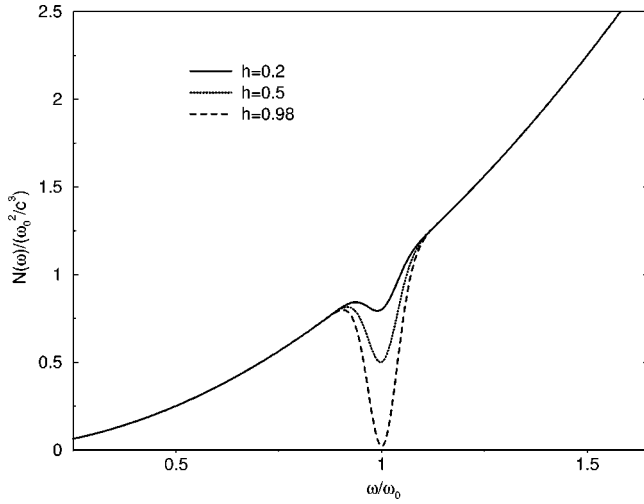


FIG. 4. Plot of the DOS [Eq. (5.8)] for the pseudogap model. The width of the gap is set by the parameter  $\Gamma=0.05\omega_0$ , which implies that the pseudogap width is 10% of its central frequency. Various depths of the pseudogap (set by  $h$ ) are shown.

tive element and the electromagnetic reservoir. This memory kernel is therefore of relevance to the description of quantum optical phenomena within a PC, as it describes the spontaneous decay contribution to the evolution of a quantum optical system.

### C. Pseudogap model

We now treat the case of a pseudogap, for which the stop band does not extend over all propagation directions, thus resulting in a suppression of the DOS rather than the formation of a full PBG. In contrast to the two cases treated above, it is not a straightforward matter to develop a model dispersion relation for a pseudogap, as this would require a more explicit treatment of the directional dependence of the photon dispersion relation. Instead, we propose a model DOS which recaptures the basic qualitative features of a pseudogap; it is plotted in Fig. 4, and has the form

$$N(\omega) = \frac{\omega^2}{c^3} \left[ 1 - h \exp\left(\frac{\omega - \omega_0}{\Gamma}\right)^2 \right]. \quad (5.8)$$

Here,  $h$  (which is dimensionless) and  $\Gamma$  (in units of  $\omega_0$ ) are parameters describing the depth and width of the pseudogap, respectively, and  $\omega_0$  is the central frequency of the pseudogap. We see that the pseudogap is assumed to have a Gaussian profile, and approaches the free space DOS away from  $\omega_0$ , i.e.,  $N(0)=0$  and  $N(\omega \gg \omega_0) = \omega^2/c^3$ . Furthermore, we obtain the free space DOS for  $h=0$ , allowing us to unambiguously compare results obtained for the pseudogap model with the corresponding values in free space. We note that this model is more realistic than the choice of a Lorentzian, whose more sharply peaked profile is better suited to describe the suppression of a single mode, rather than the suppression of the range of frequencies contained within a pseudogap.

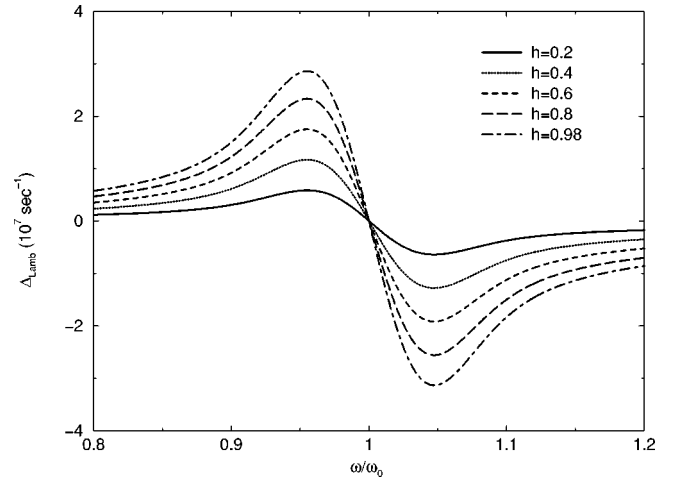


FIG. 5. Plot of the difference between the pseudogap Lamb shift and the free space Lamb shift,  $\Delta_{Lamb}$  for system parameters  $\gamma = 10^8 \text{ sec}^{-1}$ ,  $\omega_{21} = 10^{15} \text{ sec}^{-1}$  and  $\Gamma = 0.05\omega_0$ . Plots for various values of  $h$  are shown.

In Fig. 5 we plot the difference between the Lamb shift computed for the pseudogap model and the free space Lamb shift  $\Delta_{Lamb}$ . We see that in the vicinity of the bare atomic frequency,  $\omega_{21} \sim \omega_0$ , the Lamb shift is frequency dependent, as was the case near the anisotropic band edge of Sec. V B. As we have preserved the correct high- and low-frequency behavior of the DOS in the present model, we can infer that the frequency variation in the Lamb shift in the band edge case is not an artifact of our band-edge model which does not possess the correct high- and low-frequency behavior. Therefore, it is clear that both pseudogap and band-edge emission phenomena cannot simply be treated by means of a Wigner-Weisskopf approximation, as has been suggested in Refs. [41].

At  $\omega_{21} = \omega_0$ , we find that the Lamb shift for the pseudogap model is identical to the free space value, independent of the values of  $h$  and  $\Gamma$ . This is attributable to the symmetry of  $N(\omega)$  about  $\omega_0$  for frequencies within the pseudogap, which negates the contribution of the pseudogap in the evaluation of the Cauchy principal-value integral, Eq. (4.9). The calculated shift may be greater or less than the free space value, depending on whether  $\omega_{21}$  is greater or less than  $\omega_0$ , and, as expected, the deviation of the pseudogap Lamb shift from the free space value increases as the strength of the pseudogap is increased by enlarging the value of  $h$ . It is interesting to note that the maximal positive and negative values of  $\Delta_{Lamb}$  for fixed values of  $\Gamma$  and  $h$  occur at the “edges” of the pseudogap, which occur at the values  $\omega_{21} = \omega_0 \pm \Gamma$ . This is clearly due to the fact that the DOS exhibits the greatest asymmetry about these frequencies, thereby giving the largest variation when performing the Cauchy principal value integration in Eq. (4.9). This fact suggests that the maximal variation of the Lamb shift from the free space value for a system exhibiting a full PBG should occur at the band edges, as we have demonstrated in the previous section. For a sufficiently strong pseudogap, the maximal

value of  $|\Delta_{Lamb}|$  may be on the order of 15% of the free space value (see Fig. 5), a difference that should be measurable using conventional measurement techniques.

Spectral and dynamical results for the pseudogap model

are presented in Figs. 6(a) and 6(b), respectively. Here, we have incorporated the free space Lamb shift into our definition of  $\omega_{21}$ , so that  $\tilde{\omega}_{21} = \omega_{21} + \Delta_{Lamb}$ . The spectrum for this case is given by the expression

$$S(\omega) \sim \frac{2\tilde{a} \left[ 1 - h \exp\left(\frac{\omega - \omega_0}{\Gamma}\right)^2 \right] (\omega/\omega_0)}{\tilde{a}^2 \left[ 1 - h \exp\left(\frac{\omega - \omega_0}{\Gamma}\right)^2 \right]^2 (\omega/\omega_0)^2 + \{[\omega - \omega_{21} + \Delta_{Lamb}(\omega/\omega_0)]/\omega_0\}^2}, \quad (5.9)$$

where  $\tilde{a} = \gamma/2\omega_0$ . The resulting spectrum is highly Lorentzian in nature, with a linewidth that depends on the DOS in the vicinity of the atomic transition. As a result, we see that there is a narrowing of the linewidth and a corresponding

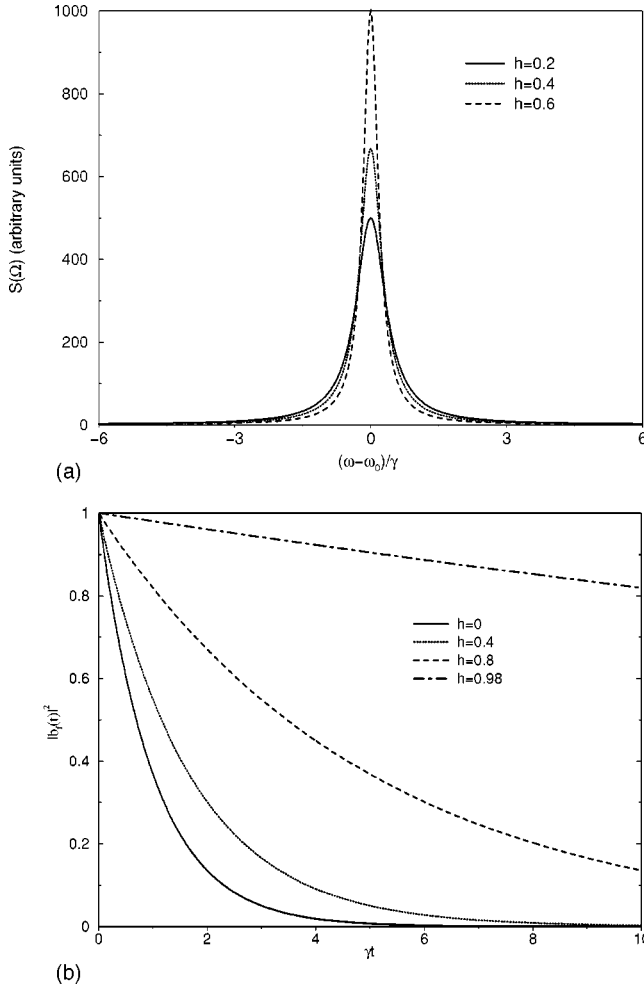


FIG. 6. (a) Emission spectrum for a two-level atom with resonant frequency coincident with the central frequency of a pseudogap,  $\omega_{21} = \omega_0$ .  $\Gamma = 0.05\omega_0$ . (b) Temporal evolution of the excited-state population for an initially excited two-level atom with resonant frequency coincident with the central frequency of a pseudogap,  $\omega_{21} = \omega_0$ .  $\Gamma = 0.05\omega_0$ . Plots for various values of  $h$  are shown.

increase in the peak of the emission spectrum for a fixed value of  $\omega_{21}$  within the pseudogap as the value of  $h$  is increased. This is in contrast to the case of an atomic transition in the vicinity of a PBG, for which the fractional localization of light in the vicinity of the emitting “atoms” means that the integrated emission intensity is not necessarily preserved as the parameters of the system are changed. As expected, the corresponding curves for the emission dynamics [Fig. 6(b)] are highly exponential, with a decay rate equal to the spectral linewidth for a given set of system parameters. We thus see that, in contrast to the case of a PBG, the spectral and dynamical characteristics of active media with radiative transitions within a pseudogap may be treated using a perturbative approach, in which we define a decay rate proportional to the DOS at the atomic resonant frequency. Such an approach is valid in the present case because of the smoothness of the DOS in our pseudogap model within the vicinity of the atomic transition frequency. A more accurate characterization of the LDOS in a strongly scattering PC, however, shows that even in the absence of a PBG, there will be a number of sharp features in the DOS and the LDOS, in particular van Hove singularities [32], whose effect on the radiative properties of an active medium cannot be described by such a perturbative treatment. Our formalism is therefore useful in obtaining a complete characterization of the present problem, including the Lamb shift, and in a broader sense allows us to describe the effect of virtually any feature of the DOS within a PC on radiative emission within the same, straightforward framework.

## VI. DISCUSSION

The formalism developed and applied in the preceding sections applies exactly to the case of a system of two-level atoms in a defect-free photonic crystal. Clearly, real systems will in general differ significantly from this idealized configuration. Any large-scale PC microfabricated at optical wavelengths will likely possess a significant number of defects, which may take the form of point defects, dislocations, and grain boundaries within the bulk of the crystal. The explicit incorporation of these effects into our formalism, though possible in principle, would be extremely computationally intensive. Qualitatively, we expect that there may be emission into directions for which photon propagation is pro-

hibited in a perfect crystal. This is a result of the scattering of radiation into the direction of a PC stop band by defects that are close enough to the crystal surface so that the scattered light passes through only a small number of crystal layers before reaching the crystal boundary, and therefore does not feel a significant Bragg scattering effect. As discussed by Megens *et al.* [18], this “defect-assisted” emission would be eliminated for an atomic transition frequency deep inside a PBG, as the active elements would not be able to emit into any direction within the bulk of the crystal. Therefore, the absence of emitted radiation at frequencies within the band gap is a strong signature of the existence of a full PBG, even in the presence of defects. It is also interesting to note that the presence of a small number of defects may actually aid in the characterization of a PC via fluorescence experiments, as the presence of defects breaks the exact mode symmetry of a given Bloch mode. This may permit us to observe emission from a Bloch mode of the crystal that may otherwise be uncoupled to externally propagating modes.

We have also made certain idealizations with respect to our description of the active medium. First, we have neglected the effects of various broadening mechanisms. The effect of a small amount of homogeneous broadening will not modify the qualitative behavior of the system, and may be minimized by considering an active medium at low temperatures. Inhomogeneous broadening effects may be introduced into our formalism by convolving our results with a probability distribution  $F(\omega)$  over the transition frequencies of the constituents of the active medium being considered. It has been pointed out that certain active media, such as organic dyes, possess both a small degree of homogeneous broadening, along with substantial inhomogeneous broadening [19]. The narrow linewidth of the individual molecules in such a dye allows one to probe the LDOS over small frequency ranges, whereas the broad distribution of emission frequencies permits one to scan the full range of frequencies for which a modification of the emission properties may be expected (for a full PBG, this may correspond to 5–20% of the midgap frequency, depending on the structure being considered). Such dyes are therefore ideal candidates for the characterization of PCs via fluorescence experiments, and their emission may be well described using our formalism.

Finally, we note that for active elements located near dielectric surfaces, and within the bulk of the dielectric, the atom-field coupling may be modified by so-called local field

effects [30,42]. These effects are a result of the microscopic interaction between individual active elements and the constituent atoms of the dielectric material, which results in a radiation reaction on the active elements. Local field effects may then serve to modify the time scales for the emission dynamics, as well as the value of the Lamb shift. Therefore, our description will apply most accurately to active elements located within the void region of a PC, away from dielectric surfaces. It is clear that each of the effects outlined above should be considered when interpreting the results of fluorescence experiments. However, such considerations do not detract significantly from the usefulness of our formalism in the characterization of fluorescence from active media in PCs.

In summary, we have developed a general formalism for the description of fluorescence from active media in photonic crystals. We have used a Bloch mode expansion of the electromagnetic field modes in order to express the fluorescence properties of the system in terms of the local density of modes available to the active elements. In the process, we have derived general expressions for the Lamb shift, emission spectrum, and emission dynamics in PCs that are readily amenable to numerical calculation in the absence of an analytic form for the local density of states. Our formalism was then applied to model densities of states in order to demonstrate the validity of the approach. Most notably, we treated the case of an anisotropic effective mass model of a photonic band edge. We showed that while this simple model provides a reasonable characterization of band-edge emission behavior, the limitations of the model motivate a more accurate determination of the band-edge density of states in order to provide a quantitatively accurate description. Finally, we have discussed how our idealized description may be modified by various effects inherent to experimental systems. The formalism presented here may find application to the characterization of photonic crystals via fluorescence experiments, as well as to the description of the interaction between an atom and the electromagnetic reservoir, which is of relevance to virtually any radiative phenomenon within a photonic crystal.

#### ACKNOWLEDGMENT

K.B. acknowledges financial support from the Deutsche Forschungsgemeinschaft under Grant No. Bu 1107/2-1 (Emmy-Noether program).

- 
- [1] *Photonic Bandgap Materials*, edited by C.M. Soukoulis, Nato Advanced Studies Institute Series E Vol. 315 (Kluwer Academic, Dordrecht, 1996).
  - [2] S. John, Phys. Rev. Lett. **53**, 2169 (1984).
  - [3] S. John, Phys. Rev. Lett. **58**, 2486 (1987).
  - [4] E. Yablonovitch, Phys. Rev. Lett. **58**, 2059 (1987).
  - [5] S. John and J. Wang, Phys. Rev. B **43**, 12 772 (1991).
  - [6] S. John and T. Quang, Phys. Rev. A **50**, 1764 (1994).
  - [7] S. John and T. Quang, Phys. Rev. Lett. **78**, 1888 (1997).
  - [8] N. Vats and S. John, Phys. Rev. A **58**, 4168 (1998).
  - [9] M. Woldeyohannes and S. John, Phys. Rev. A **60**, 5046 (1999).
  - [10] S. Noda, K. Tomoda, N. Yamamoto, and A. Chutinan, Science **289**, 604 (2000).
  - [11] P. Villeneuve, S. Fan, and J.D. Joannopoulos, Phys. Rev. B **54**, 7837 (1996).
  - [12] N. Vats and T. Rudolph, J. Mod. Opt. **48**, 1495 (2001).
  - [13] E. Yablonovitch, T.J. Gmitter, and K.M. Leung, Phys. Rev. Lett. **67**, 2295 (1991).
  - [14] J.G. Flemming and S.Y. Lin, Opt. Lett. **24**, 49 (1999).
  - [15] J.E.G.J. Wijnhoven and W.L. Vos, Science **281**, 802 (1998);

- M.S. Thijssen, R. Sprik, J.E.G.J. Wijnhoven, M. Megens, T. Narayanan, A. Lagendijk, and W.L. Vos, *Phys. Rev. Lett.* **83**, 2730 (1999).
- [16] A. Blanco, E. Chomski, S. Grabtchak, M. Ibisate, S. John, S.W. Leonard, C. Lopez, F. Meseguer, H. Miguez, J.P. Mondia, G.A. Ozin, O. Toader, and H.M. van Driel, *Nature (London)* **405**, 437 (2000).
- [17] E.P. Petrov, V.N. Bogomolov, I.I. Kalosha, and S.V. Gaponenko, *Phys. Rev. Lett.* **81**, 77 (1998).
- [18] M. Megens, J.E.G.J. Wijnhoven, A. Lagendijk, and W.L. Vos, *J. Opt. Soc. Am. B* **16**, 1403 (1999).
- [19] M. Megens, J.E.G.J. Wijnhoven, A. Lagendijk, and W.L. Vos, *Phys. Rev. A* **59**, 4727 (1999).
- [20] H.P. Schriemer, H.M. van Driel, A.F. Koenderink, and W.L. Vos, *Phys. Rev. A* **63**, 011801(R) (2001).
- [21] K. Sakoda, *Phys. Rev. B* **55**, 15 345 (1997).
- [22] U. Gruning, V. Lehmann, S. Ottow, and K. Busch, *Appl. Phys. Lett.* **68**, 747 (1996).
- [23] A. Polman, G.N. van den Hoven, J.S. Custer, J.H. Shin, R. Serna, and P.F.A. Alkemade, *Appl. Phys. Lett.* **77**, 1256 (1995); M.J.A. de Dood, L.H. Sloof, T.M. Hensen, D.L.J. Vossen, A. Moroz, T. Zijlstra, E.W.J.M. van der Drift, A. van Blaaderen, and A. Polman, in *Photonic Crystals and Light Localization*, Proceedings NATO Advanced Study Institute, Greece, 2000 (Kluwer Academic, Dordrecht, in Press).
- [24] G. Kweon and N.M. Lawandy, *Opt. Commun.* **118**, 388 (1995).
- [25] K. Busch, N. Vats, S. John, and B.C. Sanders, *Phys. Rev. E* **62**, 4251 (2000).
- [26] See, for example, F. Mandl and G. Shaw, *Quantum Field Theory* (Wiley, Toronto, 1984).
- [27] R. Sprik, B.A. van Tiggelen, and A. Lagendijk, *Europhys. Lett.* **35**, 265 (1996).
- [28] N.W. Ashcroft and N.D. Mermin, *Solid State Physics* (Harcourt Brace, Toronto, 1976).
- [29] W.H. Louisell, *Quantum Statistical Properties of Radiation* (Wiley, New York, 1973).
- [30] J.M. Wylie and J.E. Sipe, *Phys. Rev. A* **30**, 1185 (1984); **2**, 2030 (1985).
- [31] A.G. Koffman, G. Kurizki, and B. Sherman, *J. Mod. Opt.* **41**, 353 (1994).
- [32] K. Busch and S. John, *Phys. Rev. E* **58**, 3896 (1998); S. John and K. Busch, *J. Lightwave Technol.* **17**, 1931 (1999).
- [33] I.S. Gradshteyn and I.M. Ryzhik, *Table of Integrals, Series, and Products* (Academic Press, Toronto, 1980).
- [34] H.A. Bethe, *Phys. Rev.* **72**, 339 (1947).
- [35] We note that by starting with a rotating wave approximation to the dipole coupling Hamiltonian, we have neglected a “co-propagating” contribution to the Lamb shift, which adds an additional term to the rhs of Eq. (4.9) with the substitution  $(\tilde{\omega}_{21} - \omega') \rightarrow (\tilde{\omega}_{21} + \omega')$  in the denominator of the integrand; see L. Allen and J.H. Eberly, *Optical Resonance and Two-Level Atoms* (Dover, New York, 1987).
- [36] Y. Yang and S. Zhu, *Phys. Rev. A* **62**, 013805 (2000).
- [37] J.E. Sipe, *Phys. Rev. E* **62**, 5672 (2000).
- [38] E.N. Economou, *Green's Functions in Quantum Physics*, 2nd ed. (Springer-Verlag, New York, 1983).
- [39] J.D. Joannopoulos, R.D. Meade, and J.N. Winn, *Photonic Crystals* (Princeton University Press, Princeton, 1995).
- [40] M. Florescu and S. John, *Phys. Rev. A* **64**, 033801 (2001).
- [41] Z.-Y. Li and Y. Xia, *Phys. Rev. B* **63**, 121305(R) (2001); *Phys. Rev. A* **63**, 043817 (2001).
- [42] F.J.P. Schuurmans, P. de Vries, and A. Lagendijk, *Phys. Lett. A* **264**, 472 (2000).
- [43] The void regions may be replaced by a material with a sufficiently low dielectric constant relative to the first material; for example a minimum dielectric ratio of  $\sim 2.8$  is required for a full PBG in an inverse opal structure. Clearly, an air-dielectric crystal will maximize this ratio.